Analysis of terrestrial and Martian volcanic compositions using thermal emission spectroscopy
2. Application to Martian surface spectra from the Mars Global Surveyor Thermal Emission Spectrometer

Victoria E. Hamilton

Department of Geological Sciences, Arizona State University, Tempe, Arizona

Michael B. Wyatt and Harry Y. McSween Jr.

Department of Geological Sciences, University of Tennessee, Knoxville, Tennessee

Philip R. Christensen

Department of Geological Sciences, Arizona State University, Tempe, Arizona

Abstract.   Atmospherically corrected thermal infrared spectra of large regions of the Martian surface from the Mars Global Surveyor Thermal Emission Spectrometer (MGS TES) previously have been interpreted to represent two general spectral classes. One class represents a basalt to basaltic andesite composition, and the other class represents a basaltic andesite to andesite composition. We have performed new linear deconvolutions of the two Martian surface type spectra with an end-member set tailored to represent volcanic rock types. Our preparatory study of laboratory spectra of terrestrial volcanic rocks (acquired at 2 cm^{-1} sampling), convolved to TES spectral sampling (10 cm^{-1}), shows little degradation in deconvolution results when compared to results acquired using the higher spectral resolution data, indicating that the deconvolution technique is valid for analyzing data at TES resolution. Our spectral fits to the Martian data agree well with previous models and do not exhibit any notable deviations from the Martian spectra that would indicate the absence of any significant end-members in our model. Modal mineralogies obtained with these new spectral fits also compare favorably (within the previously stated uncertainties) to prior results. The newly derived modal mineralogies are used with new and traditional classification schemes for volcanic igneous rocks (introduced in a companion paper [*Wyatt et al.*, this issue]) to classify the Martian compositions. Our results substantiate the previously proposed hypothesis that these two spectral classes on the Martian surface represent volcanic compositions with distinguishable differences in silica content ranging from basalt to andesite.

1.   Introduction

As described in a companion paper [*Wyatt et al.*, this issue] (henceforth referred to as paper 1), modal mineralogies are difficult to obtain for volcanic igneous rocks, which are usually fine-grained. Therefore volcanic rocks, such as basalt and andesite, are typically distinguished and named on the basis of bulk silica and alkali oxide contents [*Le Bas et al.*, 1986]. However, although bulk chemistries of rocks are straightforward to acquire when a hand sample is available, they are much more difficult to obtain if the sample of interest can only be measured using remote-sensing techniques.

Currently in Martian orbit, the Mars Global Surveyor Thermal Emission Spectrometer (MGS TES) is acquiring thermal infrared spectra of Mars for the purpose of mapping surface geology. Because thermal infrared emissivity spectra (including those returned by the TES) are typically interpreted via linear deconvolution [*Hamilton et al.*, 1997; *Ramsey and Chris-

tensen, 1998; *Feely and Christensen*, 1999; *Hamilton and Christensen*, 2000; *Christensen et al.*, 2000a, 2000b; *Bandfield et al.*, 2000a], a technique which provides modal mineralogies rather than chemistries, classification schemes for volcanic rocks based on mineralogy, or chemistry derived from mineralogy is necessary. Paper 1 details the use of a specially selected end-member set for the linear deconvolution of thermal infrared spectra of 32 terrestrial volcanic samples, examines the accuracy of deconvolved modal mineralogies and chemistries, and discusses the use of the deconvolution results with several traditional and new classification schemes for sample identification. Although no single classification scheme is 100% accurate in classifying all samples, two or more schemes used in concert can be used to classify a rock based on its thermal infrared spectrum [*Wyatt et al.*, this issue].

In this work, we examine the effects of reducing the spectral resolution of the terrestrial rock sample data (to that of the TES instrument) on the modeled spectra, modal mineralogies, and chemistries. We then present new linear deconvolution analyses of the two Martian surface type spectra of *Bandfield et al.* [2000a] based on the end-member set presented in paper 1. Finally, we discuss the identification and discrimination of the

Martian spectra based on the new linear deconvolution results, using the classification techniques described by *Wyatt et al.* [this issue].

2. Data and Methods

2.1. Laboratory Rock and Mineral Spectra

Thermal infrared (2000–400 cm^{-1}, or ~5–25 μm) emission spectra of 32 terrestrial volcanic rocks were acquired at 2 cm^{-1} sampling with Arizona State University's (ASU) Mattson Cygnus 100 fourier transform infrared (FTIR) interferometric spectrometer [*Ruff et al.*, 1997]. Although the TES instrument covers an additional portion of the spectrum, from 400 to 200 cm^{-1} (25–50 μm), we were unable to cover this region in the laboratory with the Mattson instrument. At the time the present work was completed, ASU's Thermal Emission Spectroscopy lab had just purchased a new spectrometer that will permit coverage of the full TES wavelength range, and we anticipate using this new spectrometer to update our study. Details of the sample mineralogies and chemistries and spectral data acquisition and calibration are presented in paper 1 [*Wyatt et al.*, this issue]. For this study the terrestrial rock spectra were convolved to the exact 10 cm^{-1} sampling of the TES. Similarly, end-member mineral spectra from the ASU spectral library (also described in paper 1) [*Christensen et al.*, 2000c] were convolved to TES resolution prior to their use in linear deconvolution models of the terrestrial and Martian spectra.

2.2. TES Martian Surface Spectra

TES spectra of the Martian surface shown in this study are the "surface type 1" and "surface type 2" spectra from *Bandfield et al.* [2000a] and represent the averages of four to seven regional, low-albedo locations. Detailed descriptions of the methodology used for separating the surface and atmospheric components in TES-measured spectra are provided by *Bandfield et al.* [2000a, 2000b] and *Smith et al.* [2000]. Calibration of the TES and instrument-related errors are described by *Christensen et al.* [2000a]. Although *Bandfield et al.* [2000a] describe the bulk mineralogy of Martian dark regions in terms of two primary components, additional local-scale variations on the surface have been identified [e.g., *Christensen et al.*, 2000b; *Hoefen et al.*, 2000; *Clark and Hoefen*, 2000; *Christensen et al.*, 2001] that were not identified in the locally averaged spectra, and it is likely that further variations will become apparent as the entire TES data set is analyzed in detail. Small-scale chemical or spatial variations are not addressed here. As new and revised results are presented, we will examine them in the context of our classification schemes.

Initial examinations of the Martian surface spectra show general matches to laboratory spectra of both particulate rock samples and linear mixtures of minerals, with no evidence for unusual particle size or environmental effects [*Christensen et al.*, 2000a]. These similarities support comparisons of Martian surface spectra with thermal emission spectra of terrestrial volcanic rocks. However, Martian surface materials analyzed by TES are thought to be sand-sized particulates [*Christensen et al.*, 2000a; *Bandfield et al.*, 2000a] not bedrock, so their spectral contrast will be less than that exhibited by our laboratory rock samples [*Ruff*, 1998; *Hamilton*, 1998; *Hamilton and Christensen*, 2000]. Thus, only for visual comparison of the Martian surface spectra and laboratory spectra (e.g., Figure 4 below), we have contrast enhanced the TES spectra by 40% to simulate solid rock spectra [*Ruff*, 1998; *Hamilton and Christensen*, 2000]. Note that contrast enhancement is a cosmetic change equally affecting the entire spectrum; it does not change the shape of spectral features and was not applied to the deconvolved TES spectra.

2.3. Linear Deconvolution

The linear deconvolution technique for emission spectra is fully described by *Ramsey and Christensen* [1998], and its application to the present work is outlined in paper 1 (section 3.3). Briefly stated, the spectrum of a rock is a linear combination of the spectra of the minerals composing the rock in proportion to their abundance [*Lyon*, 1965; *Christensen et al.*, 1986; *Crown and Pieters*, 1987; *Thomson and Salisbury*, 1993]. A linear deconvolution algorithm uses a library of pure mineral spectra ("end-members") to perform a linear least squares fit to the spectrum of an unknown mixture, such as a rock [*Ramsey and Christensen*, 1998]. Upon obtaining a fit to the unknown spectrum, the algorithm supplies the user with a model-derived spectrum and the specific end-members used in the fit along with the percentage of the model represented by each end-member. The percentages are based on areal abundances (as measured by the spectrometer) and are thus comparable to percentages obtained by viewing a rock in thin section; therefore percentages are reported as vol %. The quality of the fit and resultant mineralogy can be judged by the degree of difference between the model-derived spectrum and the unknown spectrum and by the root-mean-square (RMS) error value provided as part of the output of the algorithm [*Ramsey and Christensen*, 1998; *Hamilton et al.*, 1997; *Feely and Christensen*, 1999; *Hamilton and Christensen*, 2000]. However, because RMS error values are valid only for comparing deconvolution runs for a given sample not the fits of different samples [*Hamilton and Christensen*, 2000; *Christensen et al.*, 2000], we have determined a more robust measure of uncertainty by calculating the standard deviation of the absolute differences between measured and modeled abundances [*Wyatt et al.*, this issue]. Commonly, a blackbody end-member (unit emissivity at all wavelengths) is included in the end-member set to account for differences in spectral contrast between the end-members and the mixture spectrum [*Hamilton et al.*, 1997; *Feely and Christensen*, 1999; *Hamilton and Christensen*, 2000]. Unlike continuum removal, the addition of a blackbody end-member does not change spectral shape; it only changes spectral contrast uniformly across a spectrum. Deconvolution results are typically normalized to remove any blackbody percentage so that mineral phases sum to ~100 vol %; this is how modal abundances are presented in this work.

2.4. Calculation of Bulk Oxides From Deconvolution Results

Bulk oxides for unknown spectra can be derived by summing the known chemistries of the end-members used in the best fit model in proportion to their modeled abundance [*Ruff*, 1998; *Hamilton*, 1998; *Hamilton and Christensen*, 2000]. The uncertainties associated with modeled bulk oxides derived from 10 cm^{-1} data were determined by calculating the 1 σ standard deviation of the absolute differences between the measured and modeled bulk oxide values [*Wyatt et al.*, this issue]; these are the uncertainties shown on all plots. Oxide values are generally reported to two significant figures but typically have associated uncertainties at the hundredths of a percent level that vary by oxide. Using these known values for each end-
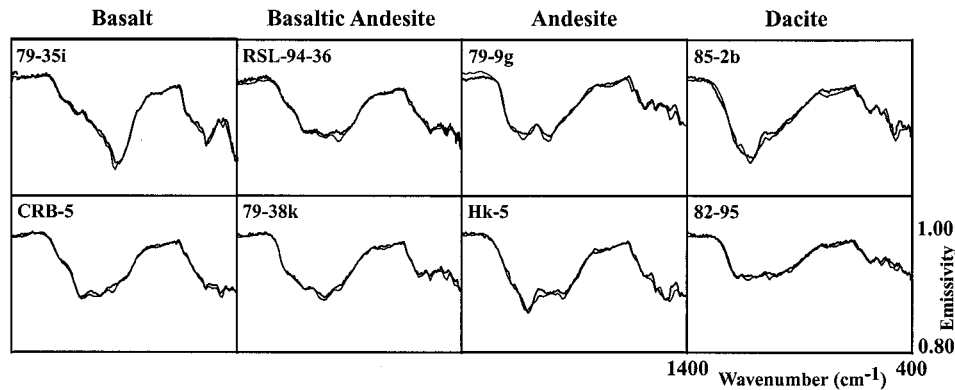
Figure 1. Example measured and modeled terrestrial rock spectra at 10 cm^{-1} spectral sampling.

member, it is possible to calculate oxides from deconvolution results to two significant figures; however, we feel that the uncertainties in the original measured values do not support reporting of more than one significant figure. Absolute abundances of different oxides in silicate rocks are widely variable but in a consistent fashion across all rocks (e.g., SiO_2 is typically ~45–75% of a rock, whereas Na_2O + K_2O is typically only ~1–8%). Therefore we also report relative uncertainties (i.e., the absolute difference divided by the measured value, multiplied by 100). Relative uncertainties are best used for determining the oxides with the greatest percentage error of the absolute quantity. Uncertainties in the deconvolved modes that might influence calculated oxide abundances are not taken into account because it is impossible to predict how variation in one or more modes would affect the modeled abundances or compositions of the remaining phases.

3. Deconvolution of Terrestrial Volcanic Compositions at Reduced Spectral Resolution

The Thermal Emission Spectrometer has selectable 5 or 10 cm^{-1} spectral sampling [*Christensen et al.*, 1992]. We resampled our laboratory rock spectra to the 10 cm^{-1} sampling of the TES and redeconvolved them to ascertain whether or not adequate results for rock classification could still be obtained with data acquired at a spectral resolution comparable to that of the lowest resolution TES data. All laboratory spectra shown in this paper are at 10 cm^{-1} sampling, and all model-derived data shown in the scatterplots are from the lower-resolution deconvolution unless otherwise stated. It is important to note that this reduction in spectral sampling does not provide an exact comparison to remotely acquired data in that the signal-to-noise ratio (SNR) of the laboratory data is higher than that of the TES and no significant atmospheric component needed to be removed; however, instrumental uncertainties [*Christensen et al.*, 2000a], sources of error associated with the atmospheric correction techniques [*Smith et al.*, 2000; *Bandfield et al.*, 2000b], and the limits of the deconvolution technique [*Ramsey and Christensen*, 1998] are extremely well known and have been used to apply a ~10–15 vol % uncertainty to the modal mineralogies obtained from TES surface spectra [*Christensen et al.*, 2000a; *Bandfield et al.*, 2000a].

Modeled spectra, modal mineralogies, and bulk rock chemistries obtained by deconvolution of the 10 cm^{-1} laboratory data show very little change from the results obtained at higher spectral resolution. Figure 1 shows example plots of several

measured and modeled terrestrial basalt, basaltic andesite, andesite, and dacite spectra. These spectra may be compared to the laboratory resolution measured and modeled spectra of the same rocks in Figures 4 and 5 of paper 1. Virtually no difference in the quality of the model fits is observable in the reduced-resolution data.

Figure 2 compares the deconvolved modal mineralogies of the terrestrial rocks obtained at 2 and 10 cm^{-1} sampling (modes have been normalized to remove blackbody components ranging from 13 to 74% [*Wyatt et al.*, this issue]). Table 1 shows the microprobe-measured modes and the 2 and 10 cm^{-1} sampling modeled modes. The uncertainty associated with the 2 cm^{-1} deconvolution results as compared to microprobe-measured modes is discussed in paper 1 and is calculated in the same way for the 10 cm^{-1} data (see section 2.3). The 1 σ standard deviation for the 10 cm^{-1} data varies by mineral group from 2.3 to 12.2 vol % (Table 2); these are
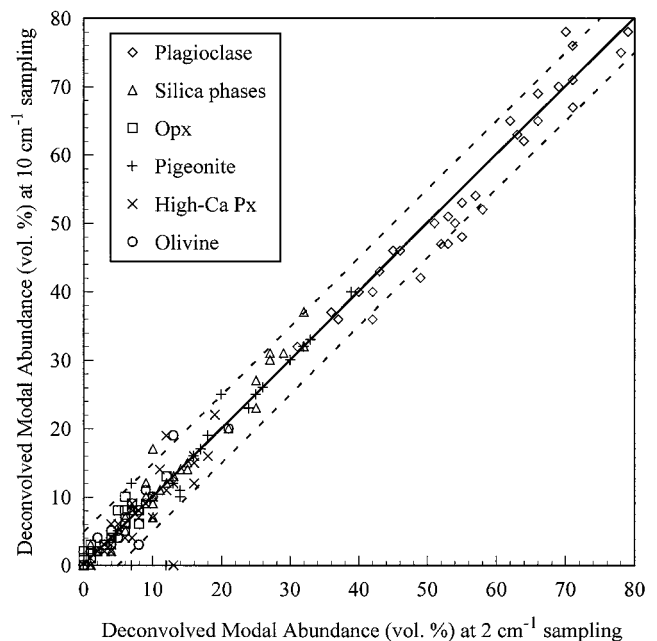
Figure 2. Scatterplot of mineral abundances deconvolved from terrestrial rock spectra at 2 versus 10 cm^{-1} spectral sampling. Dashed lines enclose points that deviate <5 vol % from the 1:1 line. Some plot points represent modes for more than one sample. Uncertainties for each phase are listed in Table 2.

Table 1. Measured and Modeled Modal Mineralogies of Laboratory Samples

Sample and Phases	Measured,[a] vol %	Modeled, vol %	
		2 cm^{-1} Sampling	10 cm^{-1} Sampling
79-35i			
Feldspar	68	71	71
Silica phases	1	0	0
Low-Ca pyroxene	0	0	0
Pigeonite	0	0	0
High-Ca pyroxene	16	7	8
Olivine	14	21	20
79-3b			
Feldspar	76	78	75
Silica phases	5	0	0
Low-Ca pyroxene	1	1	2
Pigeonite	5	0	0
High-Ca pyroxene	8	10	10
Olivine	1	6	7
HCC4E			
Feldspar	48	52	47
Silica phases	12	1	0
Low-Ca pyroxene	0	0	1
Pigeonite	4	25	25
High-Ca pyroxene	31	19	22
Olivine	3	2	2
HCC4A			
Feldspar	48	57	54
Silica phases	11	5	5
Low-Ca pyroxene	0	0	0
Pigeonite	5	7	12
High-Ca pyroxene	29	18	16
Olivine	3	0	0
79-39d			
Feldspar	46	42	36
Silica phases	39	32	37
Low-Ca pyroxene	2	8	6
Pigeonite	4	0	0
High-Ca pyroxene	5	1	0
Olivine	1	9	9
HK-1			
Feldspar	53	51	50
Silica phases	37	15	15
Low-Ca pyroxene	1	7	9
Pigeonite	3	13	12
High-Ca pyroxene	3	8	7
Olivine	0	6	6
HK-3			
Feldspar	56	55	53
Silica phases	26	12	12
Low-Ca pyroxene	5	12	13
Pigeonite	8	5	5
High-Ca pyroxene	3	9	9
Olivine	0	6	6
HK-5			
Feldspar	53	53	51
Silica phases	25	13	13
Low-Ca pyroxene	8	8	8
Pigeonite	3	18	19
High-Ca pyroxene	6	3	3
Olivine	1	6	6
82-98			
Feldspar	39	46	46
Silica phases	49	27	31
Low-Ca pyroxene	4	5	8
Pigeonite	2	7	0
High-Ca pyroxene	3	6	4
Olivine	0	8	8

[a]Feature scan (microprobe) modes are from *Wyatt et al.* [this issue].

virtually the same values that were calculated for the 2 cm^{-1} data [*Wyatt et al.*, this issue], which demonstrates that convolution to 10 cm^{-1} spectral sampling does not noticeably alter the uncertainty associated with the derived mineralogy. Therefore, as in the case of the 2 cm^{-1} data (see paper 1), the greatest uncertainties in the 10 cm^{-1} data are associated with the silica phases and pigeonite.

Modal abundances obtained from 10 cm^{-1} data commonly differ slightly from those obtained with 2 cm^{-1} data but generally not by more than 5 vol % (absolute). A few outliers are present (Figure 2), most notably three points that represent five cases in which pigeonite or clinopyroxene phases that were identified in 2 cm^{-1} data were not identified in the 10 cm^{-1} data. For two of these points the abundance of pigeonite determined from data acquired at 2 cm^{-1} sampling was <10 vol %, which is at or below the detectability limits usually associated with data acquired at 10 cm^{-1} data [*Bandfield et al.*, 2000a; *Hamilton and Christensen*, 2000]. One of the rock samples has deconvolved mineralogies at both 2 and 10 cm^{-1} sampling that include significant amounts of weathering products; this sample simply may not be modeled very accurately in either case as only a few weathering products were included in the end-member set. Finally, in the last two cases, pigeonite was not detected in the 10 cm^{-1} data at ~12 vol % (2 cm^{-1} data), but the clinopyroxene content was higher in the 10 cm^{-1} data, suggesting that the spectrum was still best modeled with a calcium-bearing pyroxene. Despite these few outlier points the similarity in the 2 and 10 cm^{-1} results indicates that the degradation of spectral resolution does not significantly alter the derived mineralogies. Therefore we expect that the chemistries derived from both data sets also will be similar.

In fact, chemistries derived from the 10 cm^{-1} spectra are very similar to those derived using the 2 cm^{-1} data. Table 2 shows the uncertainties in the 10 cm^{-1} data compared to the same values for the 2 cm^{-1} data. As an example of the consistency of our results, we have plotted the SiO$_2$ contents derived from the 2 and 10 cm^{-1} laboratory samples against the rocks' known SiO$_2$ abundances in Figure 3. The minimum and maximum absolute difference between 2 and 10 cm^{-1} modeled values are 0.1 and 2.3 wt %, respectively, with an average of only 0.5 wt %. Although bulk SiO$_2$ content is the most highly derived (model dependent) measure of composition in our studies, it is also one of the most accurate in terms of classifying the rocks [*Wyatt et al.*, this issue]. Therefore it is a good measure of the similarity and accuracy of the high- and low-resolution model results. As in the case of the 2 cm^{-1} data, the worst relative errors are observed for TiO$_2$ (95%) and MgO (85%) (Table 2); however, neither of these oxides is used in any of our classification schemes.

In summary, degradation of the laboratory rock spectra to the spectral sampling of the TES instrument does not significantly alter the mineralogies and chemistries derived by linear deconvolution of the spectra. This result demonstrates that the traditional and new classification schemes of *Wyatt et al.* [this issue] are valid for the interpretation of TES-resolution data. The following discussion examines new deconvolution results for the TES Martian surface spectra in the context of the classification schemes discussed in paper 1.

4. Martian Surface Compositions

Christensen et al. [2000a] identified a basaltic surface component in Cimmeria Terra, and *Bandfield et al.* [2000a] iden-

Table 2. Uncertainties Associated With Derived Modal Abundances and Bulk Oxides[a]

Phase	Phase Standard Deviation, vol %		Oxide	Oxide Standard Deviation, vol %		Relative Uncertainty, %	
	2 cm^{-1}	10 cm^{-1}		2 cm^{-1}	10 cm^{-1}	2 cm^{-1}	10 cm^{-1}
Plagioclase	2.9	3.1	SiO_2	1.4	1.5	3.2	3.5
Si-K_2O glass	12.2	12.2	TiO_2	0.9	0.9	94.7	95.0
Si Glass	4.8	5.2	Al_2O_3	1.5	1.7	13.0	11.3
Quartz	2.4	3.1	FeO(T)	1.2	1.2	24.2	25.3
Opx	3.1	3.3	MgO	2.6	2.4	74.5	85.2
Pigeonite	6.9	6.9	CaO	0.7	0.8	12.4	13.5
High-Ca Px	3.7	3.7	Na_2O	0.4	0.4	12.3	14.4
Olivine	2.4	2.3	K_2O	0.4	0.4	44.1	46.8
Silica phases[b]	7.2	7.2	$Na_2O + K_2O$	0.5	0.5	N/A	N/A

[a]N/A indicates information not available.

[b]Silica phases includes Si-K_2O glass, Si glass, and quartz; the standard deviation was calculated based on the sum of the knowns as if they were a single phase.

tified two primary Martian lithologies on a global scale, one basaltic to basaltic andesite (surface type 1) and another resembling basaltic andesite to andesite (surface type 2). The two Martian surface compositions are split in their distribution roughly along the planetary dichotomy that separates the ancient, heavily cratered crust in the south from younger plains in the north [*Bandfield et al.*, 2000a].

Because the results of *Christensen et al.* [2000a] and *Bandfield et al.* [2000a] were based on deconvolutions that used different sets of mineral end-member spectra than those used in this study and may not be directly comparable, we wanted to deconvolve the surface spectra obtained by *Bandfield et al.* [2000a] with the end-member set presented in paper 1. The results we obtain will necessarily differ slightly from those obtained with other end-member sets; however, this approach allows us to make the most consistent comparison to the terrestrial data provided in paper 1. Furthermore, we will be able to provide an example of the minor variability that can be expected in deconvolution results in cases in which different

end-member sets are used to deconvolve the same unknown spectrum.

It is important to note that the deconvolved mineralogies reported by *Christensen et al.* [2000a], *Bandfield et al.* [2000a], and the derived mineralogies and chemistries presented here are based on preliminary derivations of Martian surface spectra, which are themselves regional averages and may not represent local variability of the Martian surface. Detailed analysis of Martian surface spectra and deconvolved mineralogies and derived chemistries using different spectral end-member sets is ongoing.
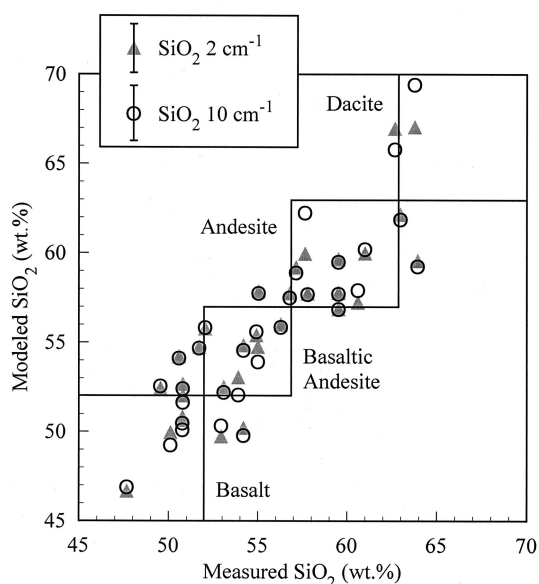
4.1. Spectral Classification

Plate 1 shows the overlapping composite spectral fields for distinguishing basalt and andesite, as described in paper 1, defined by terrestrial rock spectra at 10 cm^{-1} sampling. The spectral field shapes are nearly identical to those obtained with the 2 cm^{-1} data (see Figure 13 of paper 1); there is slightly less detail in small spectral curves and peak shapes, but the overall spectral shapes are not noticeably different. Also included in Plate 1 are the Martian surface spectra derived by *Bandfield et al.* [2000a]. The surface type 1 spectrum lies within the field defined by terrestrial basalts (the small deviation near 1250 cm^{-1} is due to a residual atmospheric CO_2 isotope band). The surface type 2 spectrum plots within or very near the terrestrial andesite field; locations where spectrum plots outside the andesite field fall within the field if the standard deviation of the surface type 2 spectrum is considered [*Bandfield et al.*, 2000a].

Christensen et al. [2000a] and *Bandfield et al.* [2000a] based the initial assessments of their spectra on comparisons to the shapes of two of our samples, WAR-R1049 (basalt) and 79-39d (andesite, see *Hamilton and Christensen* [2000] and *Wyatt et al.* [this issue] for details regarding these samples). The similarities between the Martian spectra and the laboratory sample spectra were cited as supporting the two differing compositions reported by *Bandfield et al.* [2000a].

4.2. Deconvolution of Martian Surface Mineralogies

Bandfield et al. [2000a] obtained modal mineralogies for their Martian surface spectra using a library of mineral end-members that represented a wide variety of phases. This wide variety minimized the chances that any major phases would be missed in the first deconvolution of these Martian spectra. The resulting model fit indicated that the Martian surface spectra

Figure 3. Scatterplot of measured versus modeled wt % SiO_2 for all terrestrial rocks at 2 and 10 cm^{-1} spectral sampling.
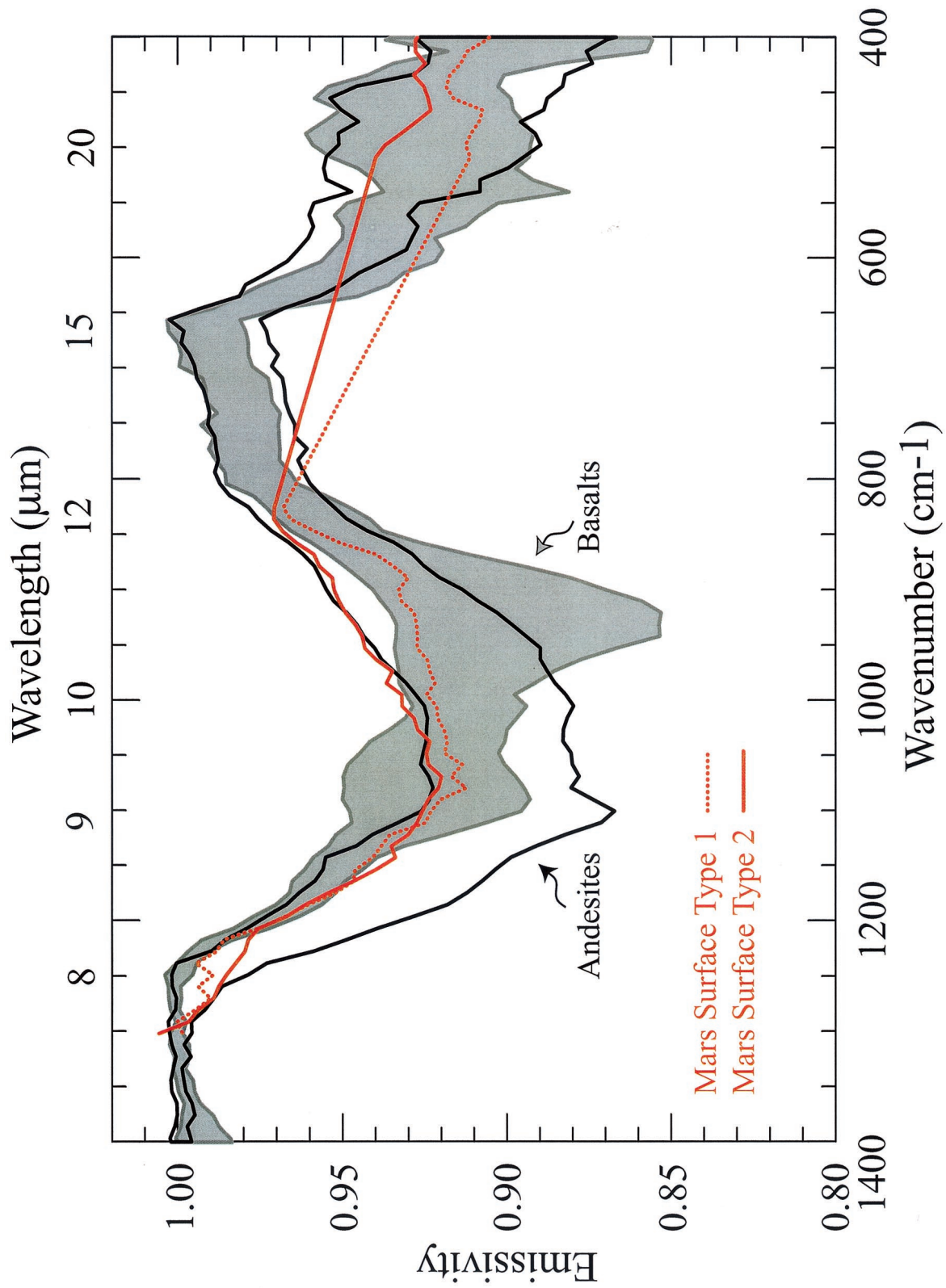
Plate 1. Martian surface spectra acquired by TES [*Bandfield et al.*, 2000a] overlaid on the spectral field classification diagram. Fields are defined by spectra of terrestrial rocks at 10 cm^{-1} sampling. Basaltic rocks fall within the gray shaded zone, and andesitic rocks lie between the black lines (the dacite fields in Figure 13 of paper 1 are not shown for clarity). Martian spectra are contrast enhanced for visual comparison only (see text for discussion).
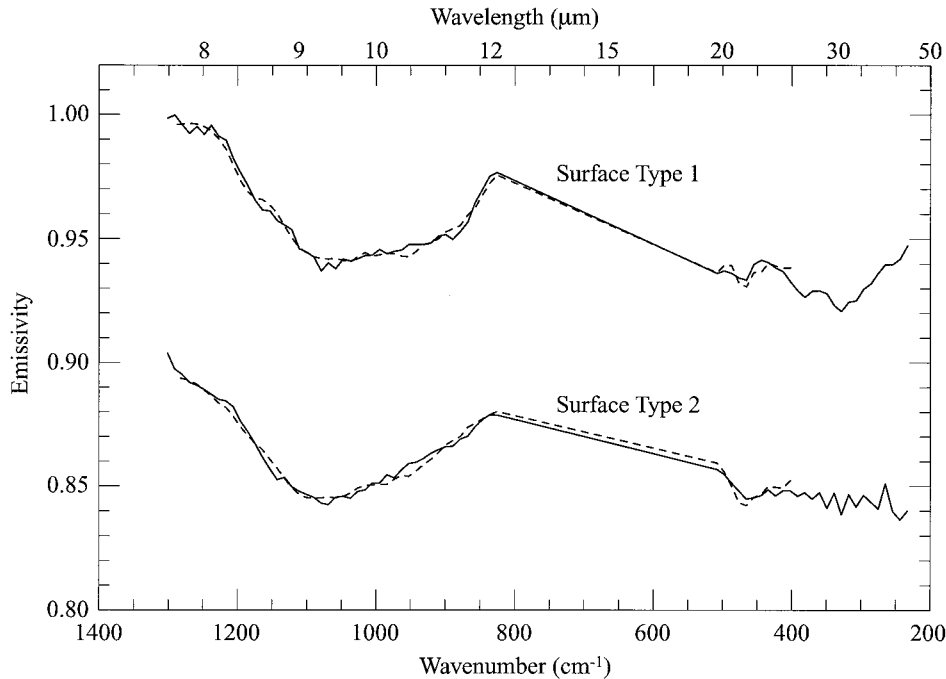
Figure 4. TES Martian surface spectra (solid lines) [*Bandfield et al.*, 2000a] and modeled spectra (dashed lines) derived using the end-member set described in paper 1 [*Wyatt et al.*, this issue]. Spectra are offset 0.1 for clarity and are not contrast enhanced.

were representative of volcanic igneous rocks, composed primarily of feldspars, pyroxenes, and glasses, with additional evidence for some sheet silicates. To apply our classification schemes to Martian data, we have performed a new deconvolution of the Martian surface spectra using our end-member set, which is tailored to the deconvolution of subalkaline volcanic compositions [*Wyatt et al.*, this issue]. This end-member set does not include the wide range of mineral groups that the *Bandfield et al.* [2000a] end-member set included, largely because the spectra can be preliminarily assigned as volcanic compositions based on their spectral signatures, but it does include an expanded range of feldspars, pyroxenes, and glasses. For consistency with previous work [*Bandfield et al.*, 2000a; *Christensen et al.*, 2000a], our model fits were performed over the spectral region from ~1280 to 400 cm^{-1}, and the region dominated by atmospheric CO_2 absorption (~825–507 cm^{-1}) was excluded. The results presented here for the Martian data should be viewed with additional sources of uncertainty in mind, such as those associated with atmospheric removal, that we cannot quantify with our laboratory data.

4.2.1. Modeled spectra. The Martian surface spectra and our modeled spectra are compared in Figure 4. The model fits are very good, with RMS values comparable (0.002) to those obtained by *Bandfield et al.* [2000a]. Our model spectra do not follow the Martian surface spectra quite as closely as the Bandfield et al. models because the Bandfield et al. fits used a greater number of end-members, with several end-members at very small abundances. These low-abundance end-members commonly are included in the fit because they can minimize slight and/or local variations between the model and the measured spectrum [*Feely and Christensen*, 1999; *Hamilton and Christensen*, 2000]. However, there are no major deviations from the measured spectrum in our modeled spectrum that

would indicate any significant components are inaccurately modeled.

4.2.2. Modal mineralogy. Modes obtained for the two Martian spectra are shown in Table 3 along with the results of *Christensen et al.* [2000a] (Cimmeria Terra) and *Bandfield et al.* [2000a] for comparison (modes have been normalized to remove blackbody components of 47 vol % [*Christensen et al.*, 2000a] and 41 and 57 vol % [this work]; blackbody percentages were not provided by *Bandfield et al.* [2000a]). Our results agree very well with the results of *Bandfield et al.* [2000a], typically well within the 10–15 vol % uncertainties of their model. Thus our results also suggest that these two surface spectra represent compositions with distinctly differing mineralogies. The most significant deviation between the two models is in the deconvolved feldspar mode for the more andesitic (surface type 2) Martian surface spectrum: we estimate ~15 vol % more feldspar than was estimated in the previous study (which is still within the uncertainty of *Bandfield et al.*, [2000a]). One possible explanation for this difference is that Bandfield et al. emphasize the abundances of major modes, which only sum to 85 vol %. The remaining modes are not discussed as they consist of end-members fit to the Martian spectrum at less than ~5 vol % and are not believed to be dependable individually because they are at or below the detection limits of the linear deconvolution technique [*Ramsey and Christensen*, 1998; *Feely and Christensen*, 1999; *Hamilton and Christensen*, 2000]. It is therefore probable that the difference in the modeled feldspar modes between these two studies is due to the difference in the end-member sets used. Owing to the reduced number of nonigneous phases in our end-member set (e.g., clays, oxides, etc.) our model fits cannot include a variety minor end-members at low abundances in the same way that the end-member set used by Bandfield et al. did. As a

Table 3. Modal Mineralogies Derived From Martian Surface Spectra[a]

Mineral Group	Cimmeria Terra/Surface Type 1: Basaltic			Surface Type 2: Andesitic	
	Christensen et al.	Bandfield et al.	This Work	Bandfield et al.	This Work
Feldspar	45	50	55	35	49
Clinopyroxene	26	25	21	(10)	
Glass			(9)	25	28
Sheet silicate	(15)	(15)	(5)	(15)	(8)
Orthopyroxene		(5)	(8)		(8)
Amphibole			(2)	(6)	(4)
Olivine	(12)			(3)	(3)
Number of end-members available	59	45	29	45	29
Number of end-members used	not stated	12	9	12	7

[a]Numbers in parenthesis are modeled at or below detection limits of ~10–15 vol % as stated by *Christensen et al.* [2000] and *Bandfield et al.* [2000].

result, the remaining (major) phases will show some reorganization and differences in the absolute abundance of each mineral group.

Although the deconvolution results of *Christensen et al.* [2000a] are for a spectrum representing only Cimmeria Terra (not shown here), we show their deconvolution results in Table 3 for general comparison with the results of *Bandfield et al.* [2000a] and this work. (Spectra from Cimmeria Terra are included in the surface type 1 of *Bandfield et al.* [2000a].) The results of our deconvolution of the basaltic (surface type 1) Martian spectrum lie within 5–10 vol % of the modes obtained by *Christensen et al.* [2000a] for the Cimmeria Terra spectrum, which is broadly similar, although not identical, in shape to the *Bandfield et al.* [2000a] surface type 1 spectrum. Therefore the results of all three studies are similar, regardless of the end-member set used and the number of end-members available.

Figure 5 shows the Martian data points on the mineralogy classification diagram from paper 1 along with the measured and derived terrestrial volcanic rock mineralogies. The modes obtained from terrestrial data convolved to 10 cm^{-1} sampling show no significant variations from data derived at 2 cm^{-1} sampling (compare to paper 1, Figure 14). Slight differences are observed in the positions of some samples but not to the extent that any rocks are reclassified; similarly, self-consistent results were obtained by *Feely and Christensen* [1999] and *Hamilton and Christensen* [2000] in their examinations of reduced-resolution deconvolution results. Mineral abundances derived from our models of the Martian surface spectra fall in the basalt and andesite fields and are consistent with the classifications based on the spectral fields in Plate 1. Even though the deconvolutions of Martian data presented by *Christensen et al.* [2000a] and *Bandfield et al.* [2000a] were performed with different end-member sets, their modal results also fall in these fields (within their uncertainties), resulting in the same classifications. These results give additional support to the basalt-basaltic andesite and basaltic andesite-andesite Martian surface compositions described by *Bandfield et al.* [2000a] as well as to applying terrestrial volcanic classification schemes from deconvolved mineralogies for distinguishing Martian surface compositions.

Our modal mineralogy (and bulk chemistry) classifications assume that glass phases identified in the deconvolution are primary volcanic phases (as they are known to be in the terrestrial samples). On the basis of currently available information (including the lack of significant quantities of weathering

products), by Occam's Razor, our interpretation is the simplest explanation of glass formation that explains the observations. If similar glasses can be demonstrated to form by secondary processes, such as oxidation [e.g., *Minitti et al.*, 2000] or acid-sulfate weathering [e.g., *Morris et al.*, 2000], and identical spectra and derived mineralogies can be obtained from samples affected by these conditions, new criteria for classifying glass-bearing surface types may be necessary.

4.3. Normative Plagioclase Composition Versus Color Index

Hamilton and Christensen [2000] and *Wyatt et al.* [this issue] have demonstrated that approximate solid-solution compositions for plagioclase feldspar and pyroxenes may be obtained
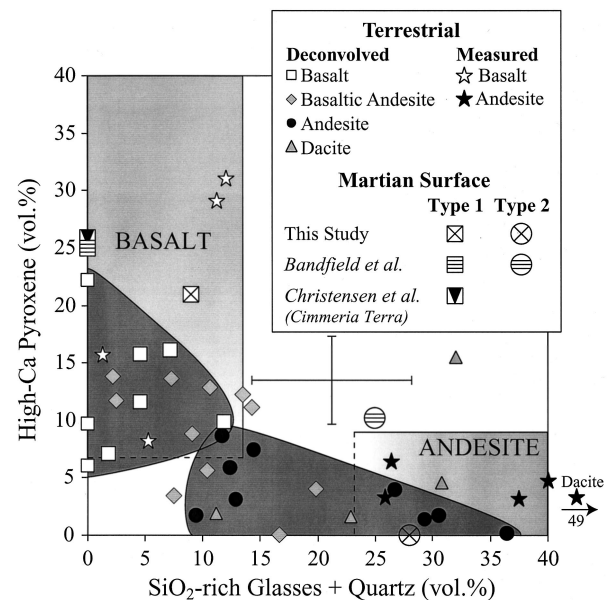
Figure 5. Modal mineralogy classification diagram from paper 1 [*Wyatt et al.*, this issue]. Terrestrial data points indicate modes derived from spectra at 10 cm^{-1} sampling. Stars represent samples with microprobe-measured modes. Error bars represent the 1 σ uncertainties listed in Table 2 for high-Ca pyroxene and silica phases. The dark shaded fields represent basaltic and andesitic fields defined only on the basis of deconvolution results of terrestrial samples and do not take into account their measured mineralogy.
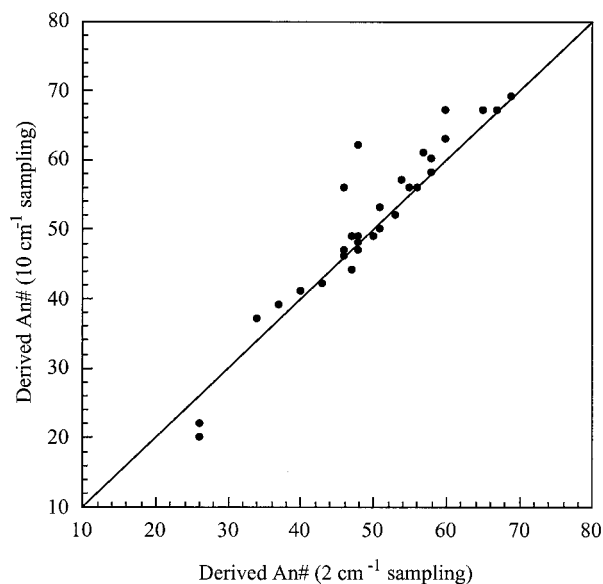
Figure 6. Comparison of average plagioclase An # derived from deconvolution of terrestrial spectra at 2 and 10 cm^{-1} sampling.

Table 4. Measured and Modeled Average Feldspar Composition

Sample	Measured An #[a]	Modeled An #	
		2 cm^{-1} Sampling	10 cm^{-1} Sampling
Basalts			
79-35i	60–85	69	69
79-3b	51–85	60	63
HCC4E	N/A	58	58
HCC4A	N/A	65	67
WAR-1049	54[b]	55	56
CRB-5	N/A	46	56
RSL-95-23	N/A	53	52
RSL-94-41	N/A	47	44
Basaltic Andesites			
CRB-4	N/A	48	48
CRB-2	N/A	48	49
CRB-6	N/A	40	41
79-24c	60–87	67	67
79-38k	45–73	47	49
79-38g	45–73	60	67
79-37j	45–70	50	49
79-4d	42–68	48	47
RSL-94-36	N/A	57	61
RSL-94-8	N/A	51	50
RSL-94-12	N/A	51	53
Andesites			
82-5	N/A	58	60
79-39d	33–70	48	62
79-9g	60–83	26	22
82-69b	N/A	54	57
HK-1	55–80	43	42
HK-3	55–80	46	46
HK-5	60–80	56	56
82-102	34–80	48	49
82-85	42–75	46	47
Dacites			
85-2b	43–75	34	37
82-88b	34–80	37	39
82-95	34–80	37	39
82-98	28–88	26	20

[a]*Wyatt et al.* [this issue].
[b]*Hamilton and Christensen* [2000].

from linear deconvolution results by taking the weighted average composition of the feldspar or pyroxene end-members used in the best fit model. The underlying assumption is that there is no single end-member spectrum that best represents the spectral character of the feldspar or pyroxene phase in the mixture spectrum; the use of several end-members within a solid solution series thus approximates the spectral signature of an intermediate composition not available in the end-member set or represents zonation in the phase [*Hamilton et al.*, 1997; *Hamilton and Christensen*, 2000]. Results are typically accurate to within 10–15 magnesium number (Mg #) or An # for mafic and ultramafic samples [*Hamilton and Christensen*, 2000] and are demonstrated to generally lie within or near the minimum and/or maximum (core and rim) microprobe-measured compositions for the mafic to silicic volcanic rocks in paper 1. Figure 6 shows a comparison of the average feldspar An # determined from the data sets at 2 and 10 cm^{-1} sampling, and the values are shown in Table 4; the derived compositions at both resolutions are very similar, typically within 0–5 An #. In the few cases that are different by >5 An #, the deconvolved values are nearly always within the core and rim values measured by electron microprobe (Table 4). Uncertainties associated with the modeled An # cannot be calculated as the volumetric average composition is not known, only the minimum and maximum An #.

Below we present the classification of our terrestrial samples and the two Martian spectra based on normative plagioclase composition (100 An/(An + Ab)) versus color index (modal olivine + orthopyroxene + clinopyroxene) [*Irvine and Baragar*, 1971]. Ongoing work by *Hamilton et al.* [2000] examines the solid-solution compositions of feldspar and pyroxene derived from deconvolution of Martian data as a function of the end-member set utilized and provides some indication of the variability possible in the derived average composition.

Figure 7 shows normative color index versus the deconvolved normative plagioclase compositions from the Martian surface spectra and the terrestrial volcanic rocks (at 10 cm^{-1} sampling) of paper 1. The uncertainty associated with norma-

tive color index was calculated in the same manner as the uncertainties in Table 2, using the sum of the mafic phases. Uncertainties for derived normative plagioclase composition cannot be calculated because we know only the range of An values, not the average compositions. As discussed in paper 1, this classification scheme is somewhat ambiguous for the terrestrial rocks in that andesites are not always accurately classified (basaltic andesites are not distinguished in this scheme), but basalts are usually correctly classified. In the case of the Martian data the two data points are plainly distinguishable, with the Martian surface type 1 spectrum plotting in the shaded basalt field and the surface type 2 spectrum plotting in the unshaded portion of the basalt field. Surface type 2 is not clearly classified using this scheme; however, this is not unexpected based on the results obtained with terrestrial samples.
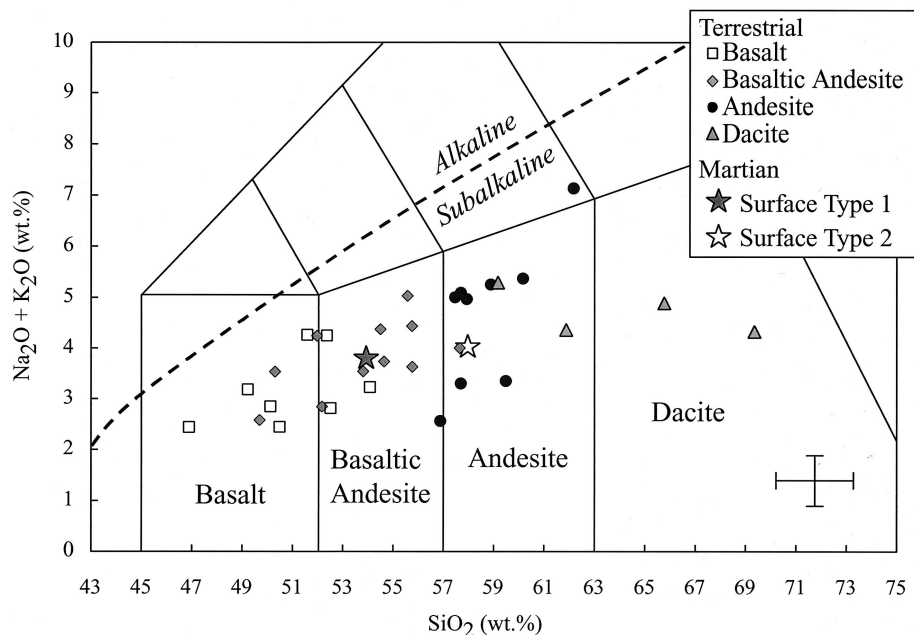
4.4. Derived Bulk Chemistries of the Martian Surface

Modal mineralogies obtained from linear deconvolution of midinfrared spectra can be converted to bulk chemistries by combining the chemistries of the spectral library end-members used in the best fit in proportion to their modeled abundances [*Hamilton*, 1998; *Ruff*, 1998; *Hamilton and Christensen*, 2000;
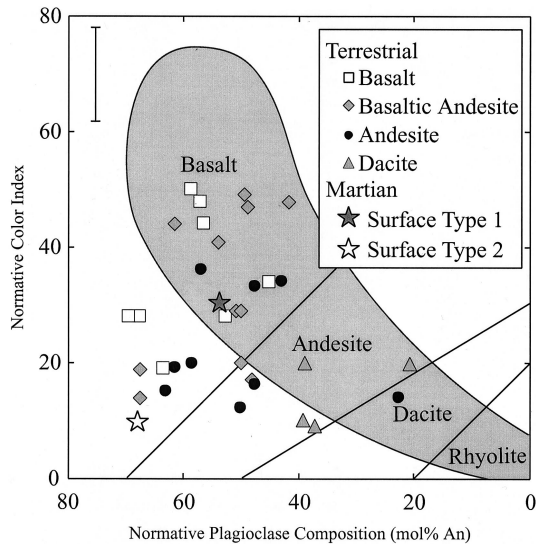
Figure 7. Normative plagioclase composition versus normative color index (both modeled) for 32 terrestrial rocks and Martian spectra (note that symbols for Martian spectra are different than in Figure 5). The shaded field represents typical terrestrial volcanic compositions [*Irvine and Baragar*, 1971]. The error bar associated with normative color index is based on the 1 σ standard deviation of the sum of the mafic phases.

Wyatt et al., this issue]. The model-derived bulk SiO_2 and alkalis ($Na_2O + K_2O$) then can be plotted on the classification diagram of *Le Bas et al.* [1986] to classify unknown samples. It is important to note, however, that model-derived chemistries are not directly representative of the chemistries of the unknown spectra; they are dependent on and represent the composition of a comparable sample composed of the exact minerals contained in the end-member set and are thus subject to slight variability as a function of the end-members selected.

Table 5. Summary of Classification Results for Martian Spectra[a]

| | Classification Schemes | | | |
Sample	Spectral Fields	Modal Mineralogy	Mineral Chemistry	Bulk Rock Chemistry
Surface type 1	B	B	B	BA
Surface type 2	A	A	B	A

[a]B, basalt; BA, basaltic andesite; A, andesite.

Figure 8 shows model-derived silica versus alkalis for the 32 terrestrial volcanic rocks of paper 1 plotted on the chemical classification scheme for volcanic rocks [*Le Bas et al.*, 1986] with our model-derived silica and alkali contents of the Martian surface spectra. Chemistries obtained from the modes derived in the present work place the *Bandfield et al.* [2000a] surface type 1 in the basaltic andesite category and surface type 2 in the andesite category. These results are consistent with the results of *Bandfield et al.* [2000a].

4.5. Summary of Classifications

The results of the four classification schemes are summarized in Table 5. Martian surface type 1 is classified as a basalt in three out of four cases, and surface type 2 is classified as an andesite in three out of four cases. This degree of consistency among the classification schemes is comparable to that obtained with terrestrial samples [*Wyatt et al.*, this issue]. These assignments agree very well with the compositional determinations of *Bandfield et al.* [2000a] and *Christensen et al.* [2000a] for surface types 1 and 2 and Cimmeria Terra.

The impact of significant abundances of weathering and alteration products is not addressed by this study, so future work is planned to investigate the impact of surface and inti-

Figure 8. Chemical classification diagram showing model-derived chemistries for terrestrial 10 cm^{-1} data and Martian spectra (stars). Symbols are the same as in Figure 7. Error bars represent the uncertainties for silica and alkalis listed in Table 2.

mate weathering and alteration phases on the determination of bulk mineralogy, chemistry, and classification. Also, the addition of data in the 400–200 cm^{-1} (25–50 μm) region will allow for a more accurate analogy to TES data and potentially will provide even better results.

5. Comparison to Martian Meteorite Compositions and Previous Results

The TES-based mineralogical results presented here and elsewhere [*Bandfield et al.*, 2000a; *Christensen et al.*, 2000a] indicate that the majority of Martian dark regions are broadly characterized by surface materials that are basaltic and andesitic in character. These results do not attempt to address local-scale variations in composition and thus do not preclude the existence of such variations. These spectra do not match known Martian meteorite spectra, are consistent with some interpretations of previously acquired data from various instruments, and are inconsistent with other previous interpretations. When considering such comparisons, it is also important to remember that different techniques are sensitive to different characteristics of the Martian surface and do not provide the same types of mineralogical information; thus some discrepancies are likely and are not necessarily problematic.

5.1. Comparison to Martian Meteorite Compositions

Martian (or shergottites, nakhlites, and chassigny (SNC)) meteorites represent lithologies ranging from basalt or lherzolite (shergottites) to clinopyroxenite (nakhlites), orthopyroxenite (ALH84001), and dunite (Chassigny). Meteorites from and within each class have clearly distinguishable thermal infrared emission spectra [*Hamilton et al.*, 1997; V. E. Hamilton, unpublished data, 2001]. The two primary surface spectral types measured by TES are not similar in shape to emission spectra of any of the Martian meteorites [*Bandfield et al.*, 2000a; *Christensen et al.*, 2000a], and the mineralogies derived from the TES spectra are not very similar to those of the Martian meteorites (summarized by *Meyer* [1998] and numerous references therein) despite the fact that surface type 1 is basaltic (as are most shergottites). We believe that this result is entirely consistent with what is known about Martian meteorites, as there are several reasons why the meteorites and their spectra should not necessarily be observed in wide distribution on the surface of Mars. First, the plutonic/cumulate nature of many of the meteorites suggests that their source regions may be at some modest depth below the surface and may not be visible at the uppermost surface, regardless of location and dust cover (see below). Second, clustering of cosmic ray exposure data suggests that a small number of craters may be responsible for all 14 Martian meteorites. The nakhlites and Chassigny share one ejection age, and the shergottites may exhibit two to three (and possibly as few as one) ejection ages on an area representing only ~15% of the Martian volcanic surface area [*Nyquist et al.*, 1998, and references therein; *Treiman*, 1995]. Therefore all of the Martian meteorites may represent as few as three ejection events (ALH84001, the nakhlites and Chassigny, and then the shergottites) if the shergottites were all ejected simultaneously [*Nyquist et al.*, 1998]. Furthermore, the likelihood of these ejection sites being clearly visible at large areal scales is decreasing as dynamical considerations of cratering events are revised. Work by *Gladman* [1997] and *Head and Melosh* [2000] has reduced the minimum crater diameter of the Martian meteorite parent craters to 3 km, which is coincident with the approximate spatial resolution of the TES instrument and below the resolution of most previous orbital instruments and telescopes (none of which have conclusively identified Martian meteorites or their source regions on Mars). On the basis of the above reasons it is not clear how representative of the uppermost Martian surface these meteorites really are, and we probably should not assume or expect that they are ubiquitous on the surface of the planet.

The TES instrument has clearly and convincingly demonstrated its ability to measure silicate and oxide minerals on the surface of Mars [*Bandfield et al.*, 2000a; *Christensen et al.*, 2000a, 2000b]. Because the spectra of the meteorites do not match the regional average spectra of the Martian surface [*Bandfield et al.*, 2000a; *Christensen et al.*, 2000a] it is reasonable to conclude that if Martian meteorite lithologies are presently exposed at the surface, they may be either limited in their areal extent or could be covered by dust. This conclusion differs from those of some previous studies [*Singer and McSween*, 1993; *Mustard et al.*, 1997] that suggested basaltic shergottites might be common on the Martian surface on the basis of visible and near-infrared (VNIR) spectra. Martian meteorites (with the exception of ALH84001) represent relatively young rocks. Geologic mapping suggests that most of the youngest rocks on Mars are in the Tharsis region [*Scott and Tanaka*, 1986]; visible images, radar, and thermal inertia data clearly demonstrate that Tharsis is among the dustiest regions on the planet as summarized by *Simpson et al.* [1992] and *Christensen and Moore* [1992]. If the meteorites' parent craters and/or units are located in Tharsis, they are quite probably covered by a thick mantle of dust that will be impenetrable to all remote-sensing instruments. In fact, many bedrock units on the surface of Mars, including the source units of the Martian meteorites, may be covered by areally extensive layers of subsequently deposited materials (e.g., dust, duricrust, or basaltic and andesitic sands) that prevent identification of bedrock lithologies. Despite all of these reasons that may help to explain why the Martian meteorites' source regions have not yet been located, TES data are still being searched for the locations of the parent regions, and local variability may provide clues to the source regions of these meteorites [e.g., *Hamilton et al.*, 2001].

5.2. Comparison to Previous Remote Sensing Results

Previous remotely acquired measurements have led to a variety of interpretations of the mineralogic composition of Martian dark regions. Visible and near-infrared spectroscopic data of some dark regions are characterized by ~1 and 2 μm absorptions that are commonly attributed primarily to the presence of ferrous (Fe^{2+}) iron in the form of pyroxene and hematite (both nanophase and crystalline) [e.g., *Adams and McCord*, 1969; *Singer et al.*, 1979; *Morris et al.*, 1989; *Mustard et al.*, 1993]. On the basis of the observation of such features, spectral signatures in Phobos-2 ISM spectra of Syrtis Major have been interpreted to represent two-pyroxene basalts similar to SNC meteorites [*Mustard and Sunshine*, 1995]. *Calvin* [1998] suggested a different perspective that attributes the observed signatures in dark regions to lesser amounts of pyroxene plus dark altered minerals that are more consistent with the observation of a 3 μm water band in intermediate- to low-albedo regions. Telescopic spectra of Acidalia Planitia by *Merényi et al.* [1996] do not exhibit a 1 μm pyroxene band (consistent with the presence of high-Ca pyroxene, olivine, mafic glass, or coatings) nor do 12 point spectra acquired by the Imager for Mars Pathfinder (which was located in a rela-

tively bright region) [*Smith et al*., 1997; *McSween et al*., 1999]. In fact, recent refinements of the APXS data acquired by Mars Pathfinder south of Acidalia Planitia indicate a silica content of ~58 wt % for soil-free rock [*Foley et al*., 2000], which is equivalent to a low-silica andesite. Thermal infrared (~8–18 μm) telescopic spectra of Acidalia Planitia analyzed by *Moersch et al*. [1997] were found to be comparable to a glassy terrestrial basalt; however, the description of the terrestrial sample as "basalt" was based on petrographic analysis not sample chemistry, and thus the term may not accurately reflect the true composition of the sample, which could be more silicic (J. Moersch, personal communication, 2001).

Our work further refines the interpretations of *Bandfield et al*. [2000a] and *Christensen et al*. [2000a], which indicate the presence of basaltic and andesitic materials in Martian dark regions. The goodness of our model fits to the two TES spectra indicates that no major components are missing in our spectral library. Current interpretations of the mineralogies represented by TES data are less consistent with some of the studies above and more consistent with others. TES-derived mineralogies for both surface types do not include low-calcium pyroxenes (orthopyroxene and/or pigeonite) at abundances above the current detectability limit for large regional averages [*Bandfield et al*., 2000a; *Christensen et al*., 2000a; this work]. However, small amounts of low-Ca pyroxenes were included in our best fit model of the surface type 1 spectrum and in the fit of *Bandfield et al*. [2000a] (8 and 5 vol %, respectively), hinting that such a component might be real, perhaps in the form of smaller local enrichments rather than as a ubiquitous component in the regional average. Additional work with individual spectra in smaller regions may provide greater confidence in the presence of this phase. Previous data also suggest that Martian surfaces may be dark and altered [*Calvin*, 1998]; TES-derived mineralogies include small amounts (~5–15 vol %) of sheet silicates [*Bandfield et al*., 2000a; *Christensen et al*., 2000a; this work]. These abundances are also at or below current detectability limits, but as in the case of low-Ca pyroxene, further studies may be able to place better constraints on the possible presence of these phases. Telescopic and in situ analyses of intermediate to dark regions in the northern hemisphere are suggestive of lesser amounts of pyroxene and more silicic (or glassy) compositions that are consistent with TES-derived mineralogies for surface type 2. In fact, the most current estimate of the silica and alkali content of the soil-free rock at the Mars Pathfinder landing site (SiO_2 = ~57.8 wt % and Na_2O + K_2O = 3.7 wt %) [*Foley et al*., 2000] is quite close to the composition derived in the present work (SiO_2 = 58.2 wt % and Na_2O + K_2O = 4.1 wt %). *Merényi et al*. [1996] observed that compositional differences in their data generally corresponded to the global crustal dichotomy of Mars, an observation similar to one previously made for the two TES surface types [*Bandfield et al*., 2000a]. The mineralogies derived from TES data thus reflect a continuum that spans many of the previously suggested compositions for Martian dark regions. Further work with smaller averages or individual spectra will surely shed light on the more subtle local variations in composition and may identify regions where some of the minerals subdued in the regionally averaged spectra are present in greater abundances.

6. Conclusions

1. Convolution of terrestrial laboratory data to the lowest spectral resolution of the TES instrument does not produce significantly degraded deconvolution results: modeled spectra provide similarly good matches to the measured spectra, modal mineralogies obtained at low (10 cm^{-1}) spectral sampling typically do not differ significantly from those obtained at high (2 cm^{-1}) spectral sampling, and bulk chemistries derived from data at reduced spectral sampling are virtually identical to those obtained from data at high spectral sampling. These results demonstrate the feasibility of using similar techniques and classification schemes for the interpretation of terrestrial laboratory samples and TES-resolution data.

2. Two distinctly different TES Martian surface spectra [*Bandfield et al*., 2000a] lie within spectral envelopes that distinguish basaltic and andesitic compositions [*Wyatt et al*., this issue], further supporting previous results indicating that these spectra represent surfaces with different mineralogies and chemistries.

3. A limited end-member set tailored to the identification of volcanic igneous rocks provides deconvolution results (modal mineralogies) for Martian spectra that are comparable to those obtained with the larger end-member sets of *Christensen et al*. [2000a] and *Bandfield et al*. [2000a]. Therefore an iterative approach to deconvolution, starting with a large set of varied end-members and working down to a smaller set of end-members that exploits solid solution variability, is justifiable.

4. The two primary Martian surface types of *Bandfield et al*. [2000a] are easily distinguished and classified here by their modal mineralogy as basaltic (surface type 1) and andesitic (surface type 2). Local-scale variations in the composition of the Martian surface were not examined but should also be distinguishable and classifiable if the variations are greater than our uncertainties. The spectra are also easily distinguished, although one (surface type 2) is not as easily classified, by their normative plagioclase composition and color index. These results are consistent with results obtained for terrestrial rock samples [*Wyatt et al*., this issue] and suggest that the plagioclase composition versus color index classification scheme should not be considered as strongly as other schemes when classifying high-silica samples. (High-silica samples can be identified by other means, such as their spectral shape and derived mineralogy.)

5. Bulk chemistries derived from our deconvolution of Martian surface spectra classify the two surface types as basaltic andesite and andesite, in general agreement with the results of previous works [*Christensen et al*., 2000a; *Bandfield et al*., 2000a].

6. In summary, the surface type 1 Martian spectrum is classified as basalt in three out of four classification schemes (the bulk chemistry scheme indicates a composition of basaltic andesite for surface type 1); we believe that this spectrum most likely represents a high-silica basaltic composition. The surface type 2 Martian spectrum is classified as andesite in three out of four classification schemes. This spectrum's mineral chemistry (color index versus plagioclase composition) plots outside the fields defined by terrestrial igneous rocks. However, this scheme is less reliable than the others in classifying deconvolved silica-rich samples [*Wyatt et al*., this issue]; therefore we believe that this spectrum is most consistent with an andesitic composition. These compositional refinements are in agreement with previously published results [*Bandfield et al*., 2000a; *Christensen et al*., 2000a].

References

Adams, J. B., and T. B. McCord, Mars: Interpretation of spectral reflectivity of light and dark regions, *J. Geophys. Res.*, *74*, 4851–4856, 1969.

Bandfield, J. L., V. E. Hamilton, and P. R. Christensen, A global view of Martian surface compositions from MGS-TES, *Science*, *287*, 1626–1630, 2000a.

Bandfield, J. L., P. R. Christensen, and M. D. Smith, Spectral dataset factor analysis and endmember recovery: Application to analysis of Martian atmospheric particulates, *J. Geophys. Res.*, *105*, 9573–9587, 2000b.

Calvin, W. M., Could Mars be dark and altered?, *Geophys. Res. Lett.*, *25*, 1597–1600, 1998.

Christensen, P. R., and H. J. Moore, The Martian surface layer, in *Mars*, edited by H. H. Kieffer et al., pp. 686–729, Univ. of Ariz. Press, Tucson, 1992.

Christensen, P. R., et al., Thermal Emission Spectrometer Experiment: Mars Observer Mission, *J. Geophys. Res.*, *97*, 7719–7734, 1992.

Christensen, P. R., J. L. Bandfield, M. D. Smith, V. E. Hamilton, and R. N. Clark, Identification of a basaltic component on the Martian surface from Thermal Emission Spectrometer data, *J. Geophys. Res.*, *105*, 9609–9621, 2000a.

Christensen, P. R., et al., Detection of crystalline hematite mineralization on Mars by the Thermal Emission Spectrometer: Evidence for near-surface water, *J. Geophys. Res.*, *105*, 9623–9642, 2000b.

Christensen, P. R., J. L. Bandfield, V. E. Hamilton, D. A. Howard, M. D. Lane, J. L. Piatek, S. W. Ruff, and W. L. Stefanov, A thermal emission spectral library of rock forming minerals, *J. Geophys. Res.*, *105*, 9735–9739, 2000c.

Christensen, P. R., R. V. Morris, M. D. Lane, J. L. Bandfield, and M. C. Malin, Global mapping of Martian hematite mineral deposits: Remnants of water-driven processes on early Mars, *J. Geophys. Res.*, in press, 2001.

Clark, R. N., and T. M. Hoefen, Spectral feature mapping with Mars Global Surveyor thermal emission spectra: Mineral implications, *Bull. Am. Astron. Soc.*, *32*(1118), abstract 62.02, 2000.

Crown, D. A., and C. M. Pieters, Spectral properties of plagioclase and pyroxene mixtures and the interpretation of lunar soil spectra, *Icarus*, *72*, 492–506, 1987.

Feely, K. C., and P. R. Christensen, Quantitative compositional analysis using thermal emission spectroscopy: Application to igneous and metamorphic rocks, *J. Geophys. Res.*, *104*, 24,195–24,210, 1999.

Foley, C. N., T. E. Economou, W. Dietrich, and R. N. Clayton, Chemical composition of Martian soil and rocks: Comparison of the results from the alpha, proton, and X-ray modes of the Pathfinder APXS, *Meteorit. Planet. Sci.*, *35*, 55–56, 2000.

Gladman, B., Destination: Earth, Martian meteorite delivery, *Icarus*, *130*, 228–246, 1997.

Hamilton, V. E., Thermal infrared emission spectroscopy of the pyroxene mineral series and pyroxene-bearing lithologies, Ph.D. dissertation, 214 pp., Ariz. State Univ., Tempe, 1998.

Hamilton, V. E. and P. R. Christensen, Determining the modal mineralogy of mafic and ultramafic igneous rocks using thermal emission spectroscopy, *J. Geophys. Res.*, *105*, 9717–9733, 2000.

Hamilton, V. E., P. R. Christensen, and H. Y. McSween Jr., Determination of Martian meteorite lithologies and mineralogies using vibrational spectroscopy, *J. Geophys. Res.*, *102*, 25,593–26,603, 1997.

Hamilton, V. E., J. L. Bandfield, and P. R. Christensen, The mineralogy of Martian dark regions from MGS TES data: Preliminary determination of pyroxene and feldspar compositions, *Lunar Planet. Sci.* [CD-ROM], *XXXI*, abstract 1824, 2000.

Hamilton, V. E., P. R. Christensen, H. Y. McSween Jr, R. N. Clark, and T. M. Hoefen, Spectral variations in MGS TES data of Nili Fossae: A possible source region for SNC meteorites on Mars?, *Lunar Planet. Sci.* [CD-ROM], *XXXII*, abstract 2184, 2001.

Head, J. N., and H. J. Melosh, Launch velocity distribution of the Martian clan meteorites, *Lunar Planet. Sci.* [CD-ROM], *XXXI*, abstract 1937, 2000.

Hoefen, T. M., R. N. Clark, J. C. Pearl, and M. D. Smith, Unique spectral features in Mars Global Surveyor thermal emission spectra: Implications for surface mineralogy in Nili Fossae, *Bull. Am. Astron. Soc.*, *32*(1118), abstract 62.03, 2000.

Irvine, T. N., and W. R. Baragar, A guide to the chemical classification of the common volcanic rocks, *Can. J. Earth Sci.*, *8*, 523–548, 1971.

Le Bas, M. J., R. W. Le Maitre, A. Streckeisen, and B. A. Zanettin, Chemical classification of volcanic rocks based on the total alkali-silica diagram, *J. Petrol.*, *27*, 745–750, 1986.

Lyon, R. J. P., Analysis of rock spectra by infrared emission (8–25 μm), *Econ. Geol.*, *60*, 715–736, 1965.

McSween, H. Y., Jr, et al., Chemical, multispectral, and textural constraints on the composition and origin of rocks at the Mars Pathfinder landing site, *J. Geophys. Res.*, *104*, 8679–8715, 1999.

Merényi, E., R. B. Singer, and J. S. Miller, Mapping of spectral variations on the surface of Mars from high spectral resolution telescopic images, *Icarus*, *124*, 280–295, 1996.

Meyer, C., Mars meteorite compendium—1998, *JSC #27672*, revision A, 237 pp., Off. of the Curator, Johnson Space Center, Houston, Tex., 1998.

Minitti, M. E., M. J. Rutherford, and J. F. Mustard, The effects of oxidation on spectra of SNC-like basalts: Applications to Mars remote sensing, *Lunar Planet Sci.* [CD-ROM], *XXXI*, abstract 1282, 2000.

Moersch, J. E., T. L. Hayward, P. D. Nicholson, S. W. Squyres, J. Van Cleve, and P. R. Christensen, Identification of a 10-μm silicate absorption feature in the Acidalia region of Mars, *Icarus*, *126*, 183–196, 1997.

Morris, R. V., D. G. Agresti, H. V. Laver Jr, H. A. Newcomb, T. D. Shelfer, and A. V. Murali, Evidence for pigmentary hematite on Mars based on optical, magnetic, and Mössbauer studies of super-paramagnetic (nanocrystalline) hematite, *J. Geophys. Res*, *94*, 2760–2778, 1989.

Morris, R. V., et al., Acid sulfate alteration products of a tholeiitic basalt: Implications for interpretation of Martian thermal emission spectra, *Lunar Planet. Sci.* [CD-ROM], *XXXI*, abstract 2014, 2000.

Mustard, J. F. and J. M. Sunshine, Seeing through the dust: Martian crustal heterogeneity and links to the SNC meteorites, *Science*, *267*, 1623–1626, 1995.

Mustard, J. F., S. Erard, J.-P. Bibring, J. W. Head, S. Hurtrez, Y. Langevin, C. M. Pieters, and C. J. Sotin, The surface of Syrtis Major: Composition of the volcanic substrate and mixing with altered dust and soil, *J. Geophys. Res.*, *98*, 3387–3400, 1993.

Mustard, J. F., S. Murchie, S. Erard, and J. M. Sunshine, In situ compositions of Martian volcanics: Implications for the mantle, *J. Geophys. Res.*, *102*, 25,605–25,615, 1997.

Nyquist, L. E., D. D. Bogard, D. H. Garrison, and Y. Reese, A single-crater origin for Martian shergottites: Resolution of the age paradox?, *Lunar Planet. Sci.* [CD-ROM] *XXIX*, abstract 1688, 1998.

Ramsey, M. S., and P. R. Christensen, Mineral abundance determination: Quantitative deconvolution of thermal emission spectra, *J. Geophys. Res.*, *103*, 577–596, 1998.

Ruff, S. W., Quantitative thermal infrared emission spectroscopy applied to granitoid petrology, Ph.D. dissertation, 234 pp., Ariz. State Univ., Tempe, 1998.

Ruff, S. W., P. R. Christensen, P. W. Barbera, and D. L. Anderson, Quantitative thermal emission spectroscopy of minerals: A laboratory technique for measurement and calibration, *J. Geophys. Res.*, *102*, 14,899–14,913, 1997.

Scott, D. H., and K. L. Tanaka, Geologic map of the western equatorial region of Mars, scale 1:15,000,000. *U.S. Geol. Surv. Misc. Invest. Ser. Map*, I-1802-A, 1986.

Simpson, R. A., J. K. Harmon, S. H. Zisk, T. W. Thompson, and D. O. Muhleman, Radar determination of Mars surface properties, in *Mars*, edited by H. H. Kieffer et al., pp. 652–685, Univ. of Ariz. Press, Tucson, 1992.

Singer, R. B., and H. Y. McSween Jr, The igneous crust of Mars: Compositional evidence form remote sensing and the SNC meteorites, in *Resources of Near-Earth space*, edited by J. S. Lewis, M. S. Matthews, and M. L. Guerrieri, pp. 709–736, Univ. of Ariz. Press, Tucson, 1993.

Singer, R. B., T. B. McCord, R. N. Clark, J. B. Adams, and R. L. Huguenin, Mars surface composition from reflectance spectroscopy: A summary, *J. Geophys. Res.*, *84*, 8415–8426, 1979.

Smith, M. D., J. L. Bandfield, and P. R. Christensen, Separation of atmospheric and surface spectral features in Mars Global Surveyor

Thermal Emission Spectrometer (TES) spectra, *J. Geophys. Res.*, *105*, 9589–9607, 2000.

Smith, P. H., et al., Results from the Mars Pathfinder Camera, *Science*, *278*, 1758–1765, 1997.

Thomson, J. L., and J. W. Salisbury, The mid-infrared reflectance of mineral mixtures (7–14 μm), *Remote Sens. Environ.*, *45*, 1–13, 1993.

Treiman, A. H., S≠NC: Multiple source areas for Maritan meteorites, *J. Geophys. Res.*, *100*, 5329–5340, 1995.

Wyatt, M. B., V. E. Hamilton, H. Y. McSween Jr, P. R. Christensen, and L. A. Taylor, Analysis of terrestrial and Martian volcanic compositions using thermal emission spectroscopy, 1, Determination of mineralogy, chemistry, and classification strategies, *J. Geophys. Res.*, this issue.

P. R. Christensen and V. E. Hamilton, Department of Geological Sciences, Box 871404, Arizona State University, Tempe, AZ 85287-1404. (hamilton@tes.la.asu.edu)

H. Y. McSween Jr and M. B. Wyatt, Department of Geological Sciences, University of Tennessee, Knoxville, TN 37996-1410. (mwyatt1@utk.edu)